https://doi.org/10.5194/egusphere-2022-1113
Preprint. Discussion started: 27 January 2023

28 years of coastal subsidence evolution on the slow-moving Nice-Côte d'Azur airport area (France) revealed by InSAR : Insights into the deformation mechanism

Olivier Cavalié[1], Frédéric Cappa[2], and Béatrice Pinel-Puysségur[3]

[1]Aix-Marseille Université, CNRS, IRD, INRAE, Coll. De France, CEREGE, Aix-en-Provence, France
[2]Université Côte d'Azur, CNRS, Observatoire de la Côte d'Azur, IRD, Géoazur, Sophia Antipolis, France
[3]CEA, DAM, DIF, Arpajon, France

Correspondence: Olivier Cavalié (cavalie@cerege.fr)

Abstract. Coastal areas can be tremendously biodiverse and host as well a substantial part of the world population and many critical infrastructures. However, there are often fragile environments and face various hazards as flooding, coast erosion, land salinization or pollution, earthquake-induced land motions, or anthropogenic processes. In this article, we investigate the stability of the Nice-Côte d'Azur airport that has been built on reclaimed land in the Var river delta (French Riviera, France). This infrastructure is a permanent concern since the partial collapse of the platform in 1979 and the on-going subsidence of the airport runways. Here, we used the full archive of ESA SAR images from 1992 to 2020 to comprehensively monitor the dynamics of the airport subsidence. We find that maximum downward motion rate is slowing down from 16 mm/yr in the 1990s to 8 mm/yr today. However, sediment compaction is still active and an acceleration phase of the continuous creep leading to a potential failure of a part of the platform cannot be excluded. Our study demonstrates the importance of remotely monitoring of the platform to better understand coastal land motions, which will ultimately help evaluate and reduce associated hazards.

1 Introduction

Global warming due to greenhouse gas emitted into the atmosphere is triggering a climate crisis whose we can already see immediate signs with more frequent extreme weather events as flooding, heatwaves or wildfires. Another consequence due to this global warming is the rise of the sea level, and the impact on the stability of coastal urban areas where a substantial part of the world's population lives. Actually, as the Earth's atmosphere get warmer, solid water (glaciers and ice sheets) melts and increases the quantity of sea water, that also occupies more volume because of thermal expansion (Wigley and Raper, 1987; Frederikse et al., 2020). Those two combined processes are inducing sea level rise (SLR) whose amplitude will depend on which Representative Concentration Pathway (RCP) emission scenario is followed. SLR is thus estimated for 2100 between 0.29 m and 0.59 m for a low emission scenario (RCP 2.6) or between 0.6 m and 1.1 m for a high emission scenario (RCP 8.5) (Oppenheimer et al., 2019). Even if the mean Earth temperature increase is kept below 2°C (compared to the pre-industrial period) within the next decades, sea level will continue to rise for several centuries or more due to the system inertia (Schaeffer et al., 2012). This estimation is worrying as UN reports that 40% of the world population live within 100 km from the coast

https://doi.org/10.5194/egusphere-2022-1113
Preprint. Discussion started: 27 January 2023

(whose more than 600 million people live in coastal areas that are less than 10 meters above sea level) and 8 of the 10 world's largest cities are near a coast.

Even if the mean Earth temperature increase is kept below 2°C (compared to the pre-industrial period) within the next decades, sea level will continue to rise for several centuries or more due to the system inertia (Schaeffer et al., 2012). It is thus important to think how cities can adapt to this long-term process as SLR has already destructive consequences. One solution is to build sea barriers. Few of them have been already built around the world to contain, locally, sudden sea water rise that occurs during extreme weather events as storms or high tides. Among the dozen of projects to impede the sea water to flood inland, we can mention one of the biggest barrier built in Venice (Italy) (Mooyaart et al., 2014). Venice is flooded regularly when high tides (acqua alta) hit the city. To protect the rich cultural heritage from the floods, a titanic project (Mose) has been implemented. It took advantage that Venice is built behind a lagoon with only four, relatively narrow ($\sim$ 400 m) openings to the Adriatic sea. A system with movable panels (flap gates) was set up to rise when high tides occur (Fice and Scotti, 1990; Mooyaart et al., 2014). The project took 18 years and 6 billion dollars (plus about 100 million $ per year for maintenance) (Kolbus, 2019). Sea barriers at larger scale don't exist yet. A famous project is the New-York Harbor storm surge barrier. But many arguments against make it very hypothetical. Among them, we can list the cost of the project, the duration (few decades), the "insiders/outsiders" dynamic, with only those behind the barriers receiving maximum protection, or the fact that the barrier could damage the zones outside its protection. But maybe the most relevant argument is just as for the Mose barrier, it won't protect the city from the long trend sea level rise.

However, sea rise is just one factor in the relative sea level changes and vertical ground motions can significantly amplify or reduce the effect of the global SLR. Indeed, sinking ground along the shoreline greatly magnifies the effects of sea level rise because both processes work together to worsen the situation (Milliman and Haq, 1996; Wöppelmann and Marcos, 2016; Wu et al., 2022). Indeed, uplift or subsidence along the coast are generated either by natural phenomena (sediment compaction (Cahoon et al., 1995), global isostatic adjustment (Farrell and Clark, 1976; Kendall et al., 2005; Peltier, 2004), or tectonics (Atwater, 1987)) or by human activities (ground water (Galloway and Burbey, 2011) or hydrocarbon extraction (Métois et al., 2020), or land reclamation (Cavalié et al., 2015)). Subsidence due to human activities are often very localized and difficult to model. They are thus often not very well known and the underlying processes remain unclear. One of the most effective method to reveal them is to measure the Earth surface displacements by InSAR (Bürgmann et al., 2000). Actually, the spatial sampling of the radar allows to map finely the location and the amplitude of these surface deformations. Indeed, the more InSAR studies, the more coastal subsidence are revealed.

In this study, we process 28 years of SAR data to obtain high-quality surface deformation time series covering the Nice Côte d'Azur airport (NCA), located in the French Riviera (southeastern France) (Figure 1a). This critical economical infrastructure (it hosted 14.485 million passengers in 2019 before the pandemic) was built in the late seventies on reclaim lands over a narrow coastal shelf (1-2 km wide). Tragically, in October 1979, during the building phase, part of the airport extension collapsed in the sea, triggering a local tsunami that caused the death of 11 people (Figure 1b). Then, part of the project was cancelled (mainly the construction of a commercial port attached to the airport) but the airport platform, which had already been completed, was

https://doi.org/10.5194/egusphere-2022-1113
Preprint. Discussion started: 27 January 2023

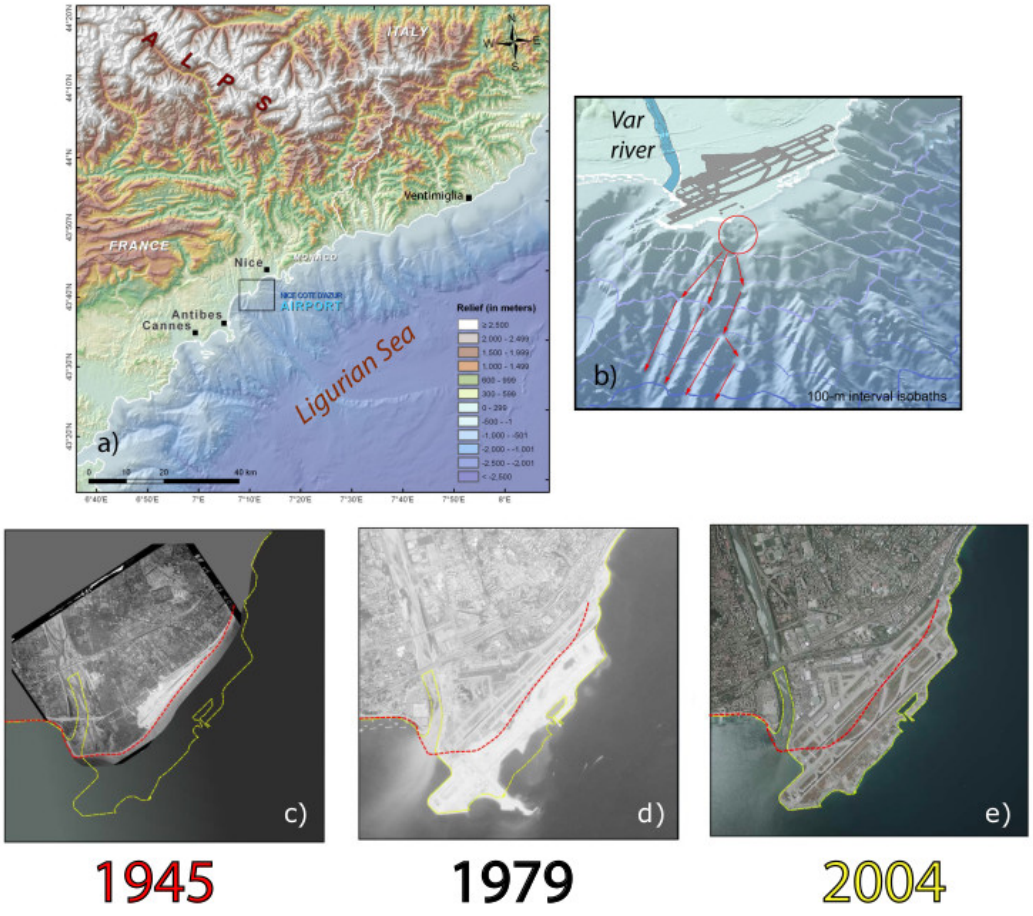

Figure 1. (a) Topographic map of the French Riviera showing the large gradient between the southern Alps and the offshore margin of the Ligurian sea (more than 4000 m elevation drop over 40 km). The black square indicates the close-up footprint shown in (b). (b) Zoom on the Nice Côte d'Azur airport with a 3-D perspective. The red circle shows the airport extension area which collapsed in 1979. The paths of the landslide are indicated with red arrows. (c-e) Three aerial photographs showing the evolution of Nice airport from the first tar runway in 1945, the maximum extension of the platform including the dyke that collapsed in October 1979, and the final shape of the airport in 2004 (it has not changed since then). On each photograph, the red and yellow dashed lines represent the coastline as it was in 1945 and 2004, respectively. (Photo credit: aerial photographies are archived by IGN and can be found at https://remonterletemps.ign.fr)

used to build the two main runways that are currently in use (Figure 1e). For hazards, it is important to measure the long term deformation of this area.

Cavalié et al. (2015) published a first study showing that between 2003 and 2011 (the acquisition period of Envisat) part of the edges of the airport was subsiding at a maximum rate of 10 mm/yr. During this period, InSAR data show essentially a steady subsidence. Here, we extended the time series in order to observe the behaviour of the airport platform over a longer

https://doi.org/10.5194/egusphere-2022-1113
Preprint. Discussion started: 27 January 2023

period (1992-2020). This provides an opportunity to investigate new mechanisms driving vertical land motion in coastal areas. Actually, no physical process could explain a constant subsidence rate over several years. We thus processed the data from the ERS satellites between 1992 and 2001 and the data acquired by Sentinel-1 for the period 2014 - 2020. Then we discussed and modelled the information brought by these new data sets. In particular, we investigated if a model of creep compaction of the airport platform can explain the data. Through our investigations, we measured a deceleration of the maximum subsidence rates of the platform from 16 mm/yr (1992-2001), then 9.5 mm/yr (2003-2011) to 8 mm/yr (2014-2020) over the study area. We find that the non-linear surface displacement can be explained by a transient creep mechanism that fits the whole temporal evolution of observations. These results are useful for future physics-based forecasting models of the coastal slope evolution.

2 History of the Airport construction

For the first half of the 20th century, Nice only hosted an aerodrome made of a single dirt track. Nice airport history really started in 1944 when the allies and the Americans set up a logistics base in Nice and thus built the first tar runway (Figure 1c). In the following years, few limited inland extensions (several hectares) of the airport platform have been done to welcome bigger planes. However, the airport is stuck between the sea and Nice city that prevents any development inland. As air traffic increased, it has been decided to extend the airport southward, on reclaimed land over sea in order to build a second runway. More than hundred of studies have been done as it is a real challenge to build there, notably because the continental shelf is very narrow (less than 2 km wide) and is bounded by very steep and deep slopes. The structural work of the platform was performed between 1975 and 1978 when 30 000 000 tons of material were brought from a neighbouring hill (Ollié, 1982). The sediments were then dynamically compacted (with a 130 kg mass falling from 22 m high). Meanwhile a 3-km long seawall have been built to protect the platform from the sea storms. In July 1978, the structural work of the airport platform was finished while construction work continued to build a dyke where a commercial port would take place. Unfortunately, the 16th of October 1979, an undersea landslide triggered the collapse of this dyke (Figure 1b,d,e). As a result, the port project got dropped, and the next three years were dedicated to consolidate the airport platform. In 1982, the last stage of the work including the construction of the pavement was achieved. The Nice airport was then inaugurated in 1983 (de la Tullaye , 1989). Since, only minor changes were added and Figure 1e shows the shape of the airport platform as it is today.

3 Data and InSAR Method

In order to extend the temporal observation window of Cavalié et al. (2015) (that spans the period 2003-2011), we processed data acquired previously by the satellites ERS and recent data acquired by the ongoing Sentinel-1 mission. The 2015 study gives important information about the deformation detected on the airport platform. In particular, it shows that the displacement is almost purely vertical (i.e., no horizontal motion stands out of the noise). So, as it is a one-dimension motion, one can process only one track and then project the line of sight (LOS) InSAR displacement into the vertical direction. For the ERS mission, the European Space Agency (ESA) clearly favored acquisitions on descending orbits for this area. We, thus, selected the track

https://doi.org/10.5194/egusphere-2022-1113
Preprint. Discussion started: 27 January 2023

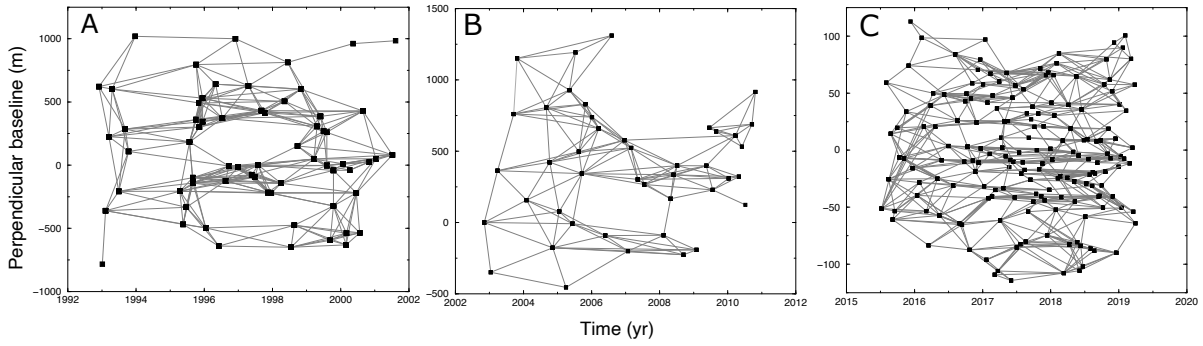

Figure 2. Relative position of orbits plotted as a function of image acquisition date for (A) descending ERS track 22, (B) descending Envisat track 22 and (C) descending Sentinel track 139. Grey lines show the interferograms included in the time series analysis.

22 where 65 images were acquired between November 1992 and September 2001 (while only 26 images are available for the ascending track over the same period). Envisat data have been already processed in Cavalié et al. (2015). For Sentinel-1 data, we processed the descending track 139. We took advantage that Sentinel SAR images are made of multiple bursts to select only those that cover the airport. As the airport is a kilometric object, only 2 bursts of the first sub-swath need to be processed.

We mostly followed the same methodology as in Cavalié et al. (2015). Ground displacement time series are generated from interferograms using the NSBAS processing chain (Doin et al., 2012). As all small baseline processing chains, the main idea consists in limiting both the temporal and spatial baseline between the images that will be combined to compute the interferograms in order to optimize the interferometric phase coherence and thus keep the highest possible number of pixels for the deformation analysis. Figure 2 shows the network of interferograms based on the image acquisition configuration for ERS, Envisat, and Sentinel-1 data. However, for ERS data, this strategy was not sufficient to reduce phase noise and we used MuLSAR software (Pinel-Puysségur et al., 2012) in order to further improve the phase stability. The principle of this software is to combine different redundant paths between acquisition dates in order to reduce the phase noise level on the wrapped interferograms.

ERS and Envisat interferograms are corrected for orbital and topographic components using DORIS and the ALOS DEM, respectively. ALOS DEM is also used to correct Sentinel-1 interferograms. To help the phase unwrapping, interferograms are filtered and slightly downsampled by pixel multilooking with 2 looks in range and 2 $\times$ 5 looks in azimuth for ERS and Envisat interferograms and 2 looks in azimuth and 2 $\times$ 4 looks in range for Sentinel-1 data. The resulting pixel spacing is ~ 40 m $\times$ 40 m. Interferograms are properly referenced using areas around the airport that has been proven to be stable (Cavalié et al., 2015). Finally, we used a constrained least-square inversion (Doin et al., 2012) in order to derive the surface displacement rates from the interferograms. A temporal smoothing operator is applied to limit phase variations due to turbulent atmospheric delays (although atmospheric delays are limited as InSAR is a relative measurement and we work at small scale). Surface velocity maps shown in Figure 3 are derived from the linear component of the time series for each pixel.

https://doi.org/10.5194/egusphere-2022-1113
Preprint. Discussion started: 27 January 2023

4 Surface displacements observed from 1992 to 2020

Figures 3a-c shows the averaged vertical ground velocity for the ERS (1992-2001), Envisat (2003-2011) and Sentinel-1 (2014-2020) periods. Note that the color scale changes to match the maximum velocity value. This representation allows to see that the spatial displacement pattern is steady through the whole observation window, although the amplitude decreases in time. This is a major update compared to the 2015's study where the time window was too short to measure reliably any slow down of the surface displacement. Thus, with this new dataset, we have the opportunity to measure subsidence rate variations over a 28 year long period of time.

To better observe the temporal variations of the airport platform subsidence, Figure 3d shows the displacement evolution of pixel P_1 that is located in the maximum subsidence area (Figure 3a). As the changes of the carrier frequency between each generation of satellites prohibit cross-interferogram (Envisat-Sentinel-1 for instance), the time series is discontinued. Thus, Figure 3d shows the three trends for each satellite period (red dots). A simple linear regression reveals that, for P_1, subsidence rates were in average 16 mm/yr, 9.5 mm/yr and 8 mm/yr for the periods 1992-2001, 2003-2011, and 2014-2020, respectively. We thus observe a deceleration of 50% of the subsidence rates over 28 years. To better visualize the evolution of the pixel displacement through the full period, one can make the assumption that no sharp motion took place between the 3 measured periods and that the shape of the motion follows a logarithmic function (with Heaviside step functions to take into account the discontinuities) :

$$f(t) = a \log\left(1 + \frac{t}{b}\right) + cH_1 + dH_2 + e \tag{1}$$

where t is the time, H_1 and H_2 are two Heaviside step functions, and a, b, c, d, and e are some constants. By inversion, one can determine them and thus reconstruct the time series (Figure 3d).

Estimating the noise level is both very important and tricky in InSAR and thus it is often either ignored in the published InSAR studies or theoretical values are given. However, several methods have been developed to estimate the noise correlation, notably to compute the InSAR data covariance matrix that are used in the inversion to retrieve parameters of the underlying geophysical phenomena (Sudhaus and Sigurjón, 2009). In the previous study (Cavalié et al., 2015), authors evaluated the uncertainties of the velocity maps by looking at the dispersion of surface velocity measurements in a nearby location where no surface displacement is expected. As a result, all velocity variations observed in the InSAR data are due to noise. Assuming that the noise level is similar on the nearby deformed area, a 1-σ error can be computed. With this method, Cavalié et al. (2015) estimated a 1-σ error of 0.25 mm/yr for the mean subsidence rate occurred between 2003 and 2011. Similarly, using the time series, one can estimate the temporal dispersion of a pixel located on a stable area. Moreover, if the temporal evolution of the surface displacement is simple enough (as it is the case for the NCA airport), one can remove a deformation model and then observe the residue dispersion. The advantage is that the 1-σ error is computed directly in the subsiding area (and not for a pixel located nearby that can be affected by other local sources of noise). Figure 4 displays the InSAR signal residue (after removing the logarithmic function estimated from Equation 1) for the pixel P_1 (shown on Figure 3a). Overall standard deviation on displacement σ_d is $\sim$4.2 mm. Interestingly, we see that data dispersion is very similar for the ERS, Envisat and Sentinel-1 time series (that have been processed independently). As in Fattahi and Amelung (2015), if we assume that the

https://doi.org/10.5194/egusphere-2022-1113
Preprint. Discussion started: 27 January 2023

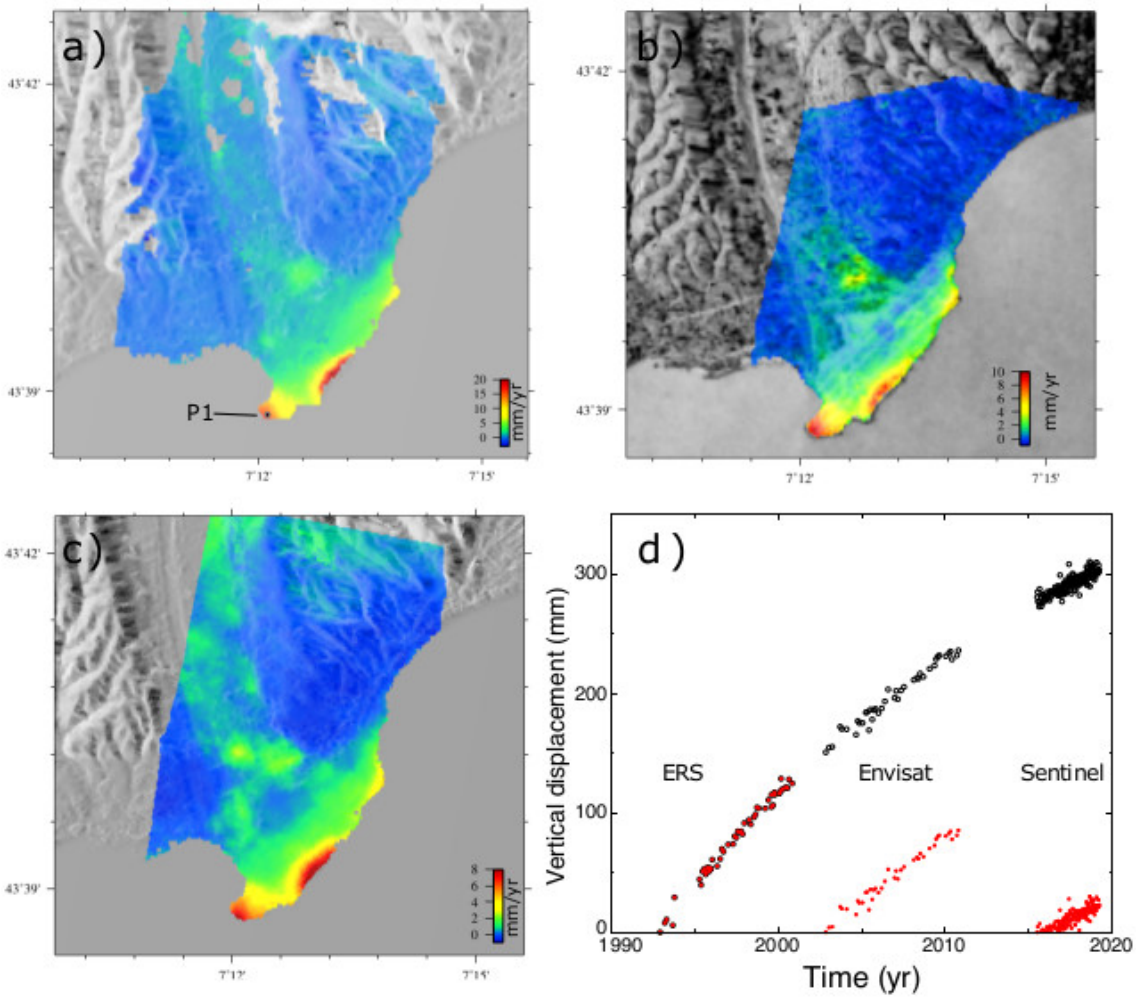

Figure 3. Projected vertical ground velocity (mm/yr) measured from (a) ERS (1992-2001), (b) Envisat (2003-2011), and (c) Sentinel-1 (2015-2020) data. Note that the color scale changes and is adapted to show the persistent patterns of deformation over time. Black dot in (a) shows the location of pixel P1. (d) Time series of P1 vertical displacement. Red dots correspond to the three times series computed independently. Black circles represent the reconstructed time series by constraining the displacement as a logarithmic function.

https://doi.org/10.5194/egusphere-2022-1113
Preprint. Discussion started: 27 January 2023

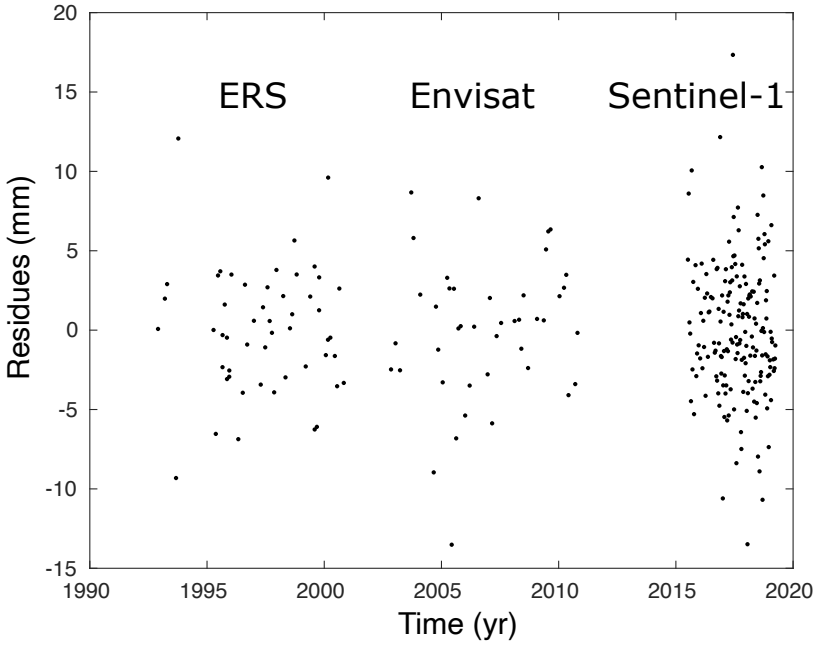

Figure 4. Displacement residues for P_1 (InSAR times series minus the fit function estimated with equation 1). Residue dispersion is ∼4.2 mm.

residue is a Gaussian white noise, the uncertainty on the deformation velocity σ_v can be estimated for each time series as:

$$\sigma_v = \frac{\sigma_d}{\sqrt{\sum_{i=1}^{N}(t_i - \bar{t})^2}} \quad (2)$$

where t_i are the acquisition dates, $\bar{t}$ is the mean acquisition date and N the number of acquisitions. σ_v is estimated to 0.27 mm/yr for ERS, 0.28 mm/yr for Envisat and 0.32 mm/yr for Sentinel-1 dataset. Interestingly, the estimate for Envisat dataset is very close to the 1-σ above mentioned error of 0.25 mm/yr estimated by a different method. Deformation velocity derived by InSAR using SBAS type techniques (Berardino et al., 2002) may be biased due to phase misclosure (De Zan et al., 2015). Recent studies suggest that this phenomenon is due to the temporal change of scattering mechanism (Ansari et al., 2021): it occurs either on vegetated areas where the scatterers vary in time due to growth or decay of the vegetation and also on bare soils where moisture level changes according to precipitation events. However, our study is focused on an urbanized area that should not be prone to this bias.

5 Creep Modelling

The time series of surface displacement data estimated from InSAR analysis shows a non-linear transient evolution over 28 years (1992 to 2020) (Figure 3d). This reflects a progressive and long-term deformation.

https://doi.org/10.5194/egusphere-2022-1113
Preprint. Discussion started: 27 January 2023

Previous studies of the submarine slope stability in the area of the Nice airport indicated that the geological formations below the airport deform with a slow creep process Dan et al. (2007); Stegmann et al. (2011). A clay layer is suspected to be the creeping section of the continental slope below the sea level and a potential contributor to the origin of submarine landslide Leynaud and Sultan (2010). Consequently, it is important to investigate the creep process to explain the slope deformation and failure. In addition, the time series of surface displacement measured from 1993 to 2019 indicates that the displacement is mainly vertical and the horizontal component is negligible. This behavior suggests that a creep compaction is probably at play.

Several models have been developed to describe creep and failure in rocks Jaeger and Cook (1979). Creep represents strain increase with time. A typical creep curve indicates three different regions: the primary, secondary and tertiary creep region (Figure 5a). Once the material experiences an instantaneous strain, as a result of sudden loading, the primary creep region begins and has a decreasing strain rate with time. This behavior continues until the secondary stage starts with a constant strain rate. The strain rate in secondary stage is the minimum strain rate of a creep deformation. The last stage of creep deformation is the tertiary creep regime characterized by very high strain rate and eventually failure.

The shape of the observed displacement at the surface of the airport is similar to the shape of the primary and secondary creep stages of the theoretical creep curve. A viscoelastic Burger's model can effectively reflect the primary and secondary creep stages of rock creep process; however, it cannot describe the acceleration phase of tertiary creep. Here, we use an extended Burger's creep model made up of a series of Maxwell and Kelvin bodies to reproduce the observations. Such viscoelastic model was previously employed to model soil deformation Yao et al. (2021), fault relaxation after earthquakes Sun and Wang (2015), landslide creep Zou et al. (2013), and is often used in geology to illustrate the effects of both strain and stress relaxation. The transient creep (δ) with time (t) is analytically calculated as follows:

$$\delta(t) = \sigma_0 \left[\frac{1}{E_M} + \frac{t}{\eta_M} + \frac{1}{E_{K_1}} \left(1 - \exp\left(-\frac{E_{K_1} t}{\eta_{K_1}} \right) \right) + \frac{1}{E_{K_2}} \left(1 - \exp\left(-\frac{E_{K_2} t}{\eta_{K_2}} \right) \right) \right] \tag{3}$$

where E_M, E_{K1}, E_{K2} are the elastic moduli of the Maxwell body, the first and second Kelvin bodies, respectively; η_M, η_{K1}, η_{K2} are the viscosity of the Maxwell body, the first and second Kelvin bodies, respectively; σ_0 is a constant uniaxial load. The transient Kelvin component of the rheology is considered to be dominant at short timescales, while the Maxwell component dominates at long timescales Jaeger and Cook (1979). With this 1D model, 7 parameters need to be adjusted. We used an adaptive grid search method to invert the parameters. We set up the search range of each parameter to explore a large number of possible solutions, that is about 2.3 million of solutions. For the goodness of fit of the best-fit solution, the misfit between the observed (obs_i) and model-predicted ($pred_i$) displacement is estimated with the reduced chi-square (χ^2), defined as:

$$\chi^2 = \frac{1}{N-m} \sum_{i=1,N} \left(\frac{\mathrm{obs}_i - \mathrm{pred}_i}{\sigma_i} \right)^2 \tag{4}$$

with N is the number of observations, m is the number of model parameters, and σ_i is the uncertainties (4.2 mm here).

https://doi.org/10.5194/egusphere-2022-1113
Preprint. Discussion started: 27 January 2023

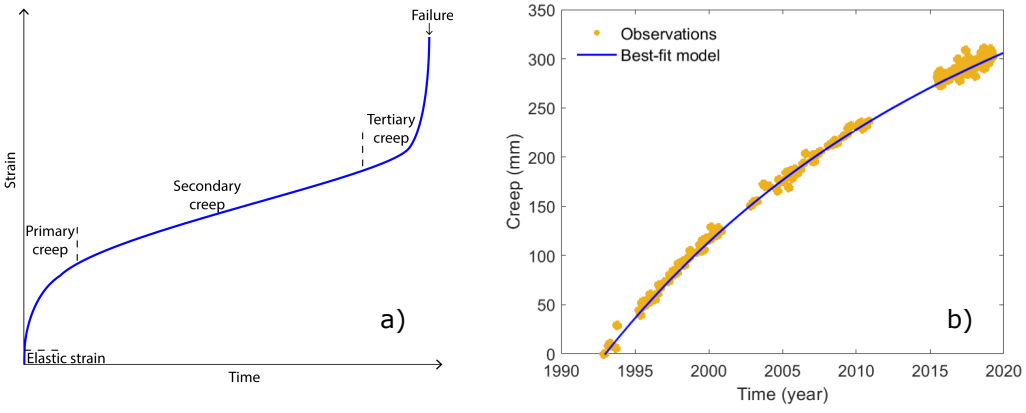

Figure 5. (a) Strain-time plot for a conventional creep experiment. On this typical creep curve, the three creep phases (primary, secondary, and tertiary) are labelled. (b) Time series of the measured displacement and the best fit numerical solution using the extended viscoelastic Burger's model. The model adjusts the data with $\chi^2 = 0.18957$.

Figure 5b shows the best fit numerical solution to the measured displacement over time. The model provides a satisfying fit of observations and adjusts the data with a reduced chi-square of 0.18957, and leads to $\sigma_0 = 0.099$ MPa, $E_M = 32.1$ MPa, $E_{K_1} = 0.86$ MPa, $E_{K_2} = 0.47$ MPa, $\eta_M = 42.63$ MPa/yr, $\eta_{K_1} = 16.21$ MPa/yr, $\eta_{K_2} = 9.61$ MPa/yr. These values are consistent with the range of values obtained in laboratory experiments conducted on clays under triaxial compression condition Xue et al. (2020). The difference between the observed and modeled displacements reflects mostly the data dispersion as we find a very similar standard deviation, 4.1 mm, for the residues (data minus model). Thus, this result suggests that a transient creep mechanism properly models our observations of the vertical displacement associated with a long-term compaction of materials. Based on this assumption, the airport deformation is still in primary stage of the creep process.

Although the data are well reproduced with an extended Burger's creep model, which allows to investigate a transient rheology for viscous compaction, an extension to a creep damage model in a three-dimensional stress state would be adapted to explore the full non-linear visco-elasto-plastic behavior with potential damage accumulation and accelerated creep (tertiary creep stage in Figure 3d) toward dramatic failure. However, the 1D viscoelastic creep model used here is well adapted to explain the data with a satisfying fit over the 28 years of observation.

6 Conclusions

In this study, we use SAR interferometry to measure and analyze the temporal evolution of the ground displacement on the Nice Côte d'Azur airport platform over a long period of 28 years. Extending the observation window to study the long-term subsidence leads to substantial improvements in the understanding of the ongoing mechanisms along this coastal area. Indeed, the previous study Cavalié et al. (2015) measured the airport platform subsidence using only the Envisat data that span the 2003-2011 period. This relative short period of observation impeded to detect accurately non-linearity of the surface displacement

https://doi.org/10.5194/egusphere-2022-1113
Preprint. Discussion started: 27 January 2023

and its change rate. By adding the ERS and Sentinel-1 data, the observation window more than tripled (1992-2020) and times series of the surface displacement clearly reveal a transient non-linear deformation with decelerating subsidence rate over time, that is expected for ground layer compaction. Then, we used a simple analytical Burger's creep model to constrain the mechanisms and rheology at play. The data are properly explained by the primary and secondary creep phases, highlighting a slow viscoelastic deformation at multiyear timescales. The best-fit solution allows to retrieve reasonable mechanical values of the airport sediments that have been brought to build the platform extension. Our study thus proves that the long-term InSAR data can improve our understanding of the surface processes and the subsurface material properties.

Although the subsidence rate decelerates since 28 years, our results show that the compaction of the sediment is still active and its future evolution is uncertain and still at stake. Indeed, if compaction zones are developing under the airport platform, creep process could potentially lead to accumulated material damage toward failure. Thus, through our investigations, the data indicates that the stability of the airport platform should be monitored continuously with additional high-quality space and land observations together with submarine instrumentation on the continental slope right below the airport. In an era in which climate change and sea-level rise pose unprecedented threats to coastal ecosystems and urbanizations Shirzaei and Burgmann (2018); Shirzaei et al. (2021), the long-term observations of ground motions from space is essential to monitor the stability of coastal environment and will inform managers and policymakers identify zones with exposure to hazards.

Data availability. Raw data used in this study are freely available online. Sentinel-1 SAR images are from the PEPS platform (https://peps.cnes.fr/rocket/#/search). ERS and Envisat SAR data were obtained free of charges through a ESA cat1 project (https://earth.esa.int/eogateway/catalog/ers-1-2-sar-im-l0-sar_im__0p- and https://earth.esa.int/eogateway/catalog/envisat-asar-im-l0-asa_im__0p-?text=envisat%20asar%20im%20l0%20%5Basa_im__0p%5D, respecively). The digital elevation model is freely available from JAXA (https://www.eorc.jaxa.jp/ALOS/en/-dataset/aw3d30/aw3d30_e.htm). ERA-5 global reanalyses of atmospheric data are distributed by the ECMWF (https://www.ecmwf.int/en/forecasts/datasets/reanalysis-datasets/era5). Velocity maps shown in Figure 3 are archived on Zenodo (https://doi.org/10.5281/zenodo.7038263).

Author contributions. OC initiated the project and processed the InSAR data with BPP's help. FC analysed the deformation in term of mechanical process and modelled the InSAR data. Everybody got involved in the writing process of the article.

Competing interests. No competing interests are present

Acknowledgements. This work was supported by CNES, focused on data provided by the European space agency (ERS, Envisat and Sentinel-1 missions).

https://doi.org/10.5194/egusphere-2022-1113
Preprint. Discussion started: 27 January 2023

References

Ansari, H., De Zan, F., and Parizzi, A.: Study of Systematic Bias in Measuring Surface Deformation With SAR Interferometry, IEEE Transactions on Geoscience and Remote Sensing, 59, 1285–1301, https://doi.org/10.1109/TGRS.2020.3003421, 2021.

Atwater, B. F.: Evidence for great Holocene earthquakes along the outer coast of Washington State, Science, 236, 942–944, 1987.

Berardino, P., Fornaro, G., Lanari, R., and Sansosti, E.: A new algorithm for surface deformation monitoring based on small baseline differential SAR interferograms, IEEE Transactions on Geoscience and Remote Sensing, 40, 2375–2383, https://doi.org/10.1109/TGRS.2002.803792, 2002.

Bürgmann, R., Rosen, P. A., and Fielding, E. J.: Synthetic Aperture Radar interferometry to measure Earth's surface topography and its deformation, Annu. Rev. Earth. Planet. Sci., 28, 169–209, 2000.

Cahoon, D. R., Reed, D. J., and Day Jr, J. W.: Estimating shallow subsidence in microtidal salt marshes of the southeastern United States: Kaye and Barghoorn revisited, Marine geology, 128, 1–9, 1995.

Cavalié, O., Sladen, A., and Kelner, M.: Detailed quantification of delta subsidence, compaction and interaction with man-made structures : the case of the NCA airport, France, Nat. Hazards Earth Syst. Sci., 15, 1–12, https://doi.org/10.5194/nhess- 15-1-2015, 2015.

Dan, G., Sultan, N., , and Savoye, B.: The 1979 Nice harbour catastrophe revisited: Trigger mechanism inferred from geotechnical measurements and numerical modelling, Mar. Geol., 245, 40–64, 2007.

de la Tullaye , M.: Nice-Côte d'Azur, un aéroport gagné sur la mer, Revue XYZ, 38, 43–45, 1989.

De Zan, F., Zonno, M., and López-Dekker, P.: Phase Inconsistencies and Multiple Scattering in SAR Interferometry, IEEE Transactions on Geoscience and Remote Sensing, 53, 6608–6616, https://doi.org/10.1109/TGRS.2015.2444431, 2015.

Doin, M.-P., Lodge, F., Guillaso, S., Jolivet, R., Lasserre, C., Ducret, G., Grandin, R., Pathier, E., and Pinel, V.: Presentation of the small baseline NSBAS processing chain on a case example: the Etna deformation monitoring from 2003 to 2010 using Envisat data, Proc. of FRINGE 2011 Workshop, Frascati, Italy, 19-23 September 2011 (ESA, SP-697, January 2012), 2012.

Farrell, W. and Clark, J.: On Postglacial Sea Level, Geophys. JR Astron. Soc., 46, 647–667, 1976.

Fattahi, H. and Amelung, F.: InSAR bias and uncertainty due to the systematic and stochastic tropospheric delay, Journal of Geophysical Research: Solid Earth, 120, 8758–8773, https://doi.org/https://doi.org/10.1002/2015JB012419, 2015.

Fice, J. L. and Scotti, A.: The Flood-Prevention Scheme of Venice: Experimental Module, Water and Environment Journal, 4, 70–77, https://doi.org/10.1111/j.1747-6593.1990.tb01559.x, 1990.

Frederikse, T., Landerer, F., Caron, L., Adhikari, S., Parkes, D., Humphrey, V. W., Dangendorf, S., Hogarth, P., Zanna, L., Cheng, L., et al.: The causes of sea-level rise since 1900, Nature, 584, 393–397, 2020.

Galloway, D. L. and Burbey, T. J.: Regional land subsidence accompanying groundwater extraction, Hydrogeology Journal, 19, 1459–1486, 2011.

Jaeger, J. C. and Cook, N. G.: Fundamentals of Rock Mechanics, Chapman and Hall, London, U.K, 1979.

Kendall, R. A., Mitrovica, J. X., and Milne, G. A.: On post-glacial sea level–II. Numerical formulation and comparative results on spherically symmetric models, Geophysical Journal International, 161, 679–706, 2005.

Kolbus, C.: MOSE: The future of Venice, engineeringrome.org, http://engineeringrome.org/2019/05/01/colin-kolbus/, 2019.

Leynaud, D. and Sultan, N.: 3-D slope stability analysis: A probability approach applied to the nice slope (SE France), Mar. Geol., 269, 89–106, 2010.

https://doi.org/10.5194/egusphere-2022-1113
Preprint. Discussion started: 27 January 2023

Métois, M., Benjelloun, M., Lasserre, C., Grandin, R., Barrier, L., Dushi, E., and Koçi, R.: Subsidence associated with oil extraction, measured from time series analysis of Sentinel-1 data: case study of the Patos-Marinza oil field, Albania, Solid Earth, 11, 363–378, 2020.

Milliman, J. D. and Haq, B. U.: Sea-level rise and coastal subsidence: Causes, consequences, and strategies, vol. 2, Springer Science & Business Media, 1996.

Mooyaart, L. F., Jonkman, S. N., De Vries, P. A., Van der Toorn, A., and Van Ledden, M.: Storm surge barrier: Overview and design considerations, in: ICCE 2014: Proceedings of 34th International Conference on Coastal Engineering, Seoul, Korea, 15-20 June 2014, Coastal Engineering Research Council, 2014.

Ollié, J.-P.: L'extension sud de l'aéroport international de Nice - Côte d'Azur. Le point sur les travaux, Revue générale des routes et des aérodromes, 1982.

Oppenheimer, M., Glavovic, B. C., Hinkel, J., van de Wal, R., Magnan, A. K., Abd-Elgawad, A., Cai, R., Cifuentes-Jara, M., DeConto, R. M., Ghosh, T., Hay, J., Isla, F., Marzeion, B., Meyssignac, B., and Sebesvari, Z.: 2019: Sea Level Rise and Implications for Low-Lying Islands, Coasts and Communities, In: IPCC Special Report on the Ocean and Cryosphere in a Changing Climate [H.-O. Pörtner, D.C. Roberts, V. Masson-Delmotte, P. Zhai, M. Tignor, E. Poloczanska, K. Mintenbeck, A. Alegría, M. Nicolai, A. Okem, J. Petzold, B. Rama, N.M. Weyer (eds.)]., 2019.

Peltier, W. R.: Global glacial isostasy and the surface of the ice-age Earth: the ICE-5G (VM2) model and GRACE, Annu. Rev. Earth Planet. Sci, 32, 2004.

Pinel-Puysségur, B., Michel, R., and Avouac, J.-P.: Multi-Link InSAR Time Series: Enhancement of a Wrapped Interferometric Database, IEEE Journal of Selected Topics in Applied Earth Observations and Remote Sensing, 5, 784–794, https://doi.org/10.1109/JSTARS.2012.2196758, 2012.

Schaeffer, M., Hare, W., Rahmstorf, S., and Vermeer, M.: Long-term sea-level rise implied by 1.5 °C and 2 °C warming levels, Nature Climate Change, 2, 867–870, https://doi.org/10.1038/nclimate1584, 2012.

Shirzaei, M. and Burgmann, R.: Global climate change and local land subsidence exacerbate inundation risk to the San Francisco Bay Area, Science Advances, 4, https://doi.org/10.1126/sciadv.aap9234, 2018.

Shirzaei, M., Freymueller, J., Törnqvist, T. E., Galloway, D. L., Dura, T., and Minderhoud, P. S. J.: Measuring, modelling and projecting coastal land subsidence, Nature Reviews Earth & Environment, 2, 40–58, https://doi.org/10.1038/s43017-020-00115-x, 2021.

Stegmann, S., Sultan, N., Kopf, A., Apprioual, R., and Pelleau, P.: Hydrogeology and its effect on slope stability along the coastal aquifer of Nice, France, Marine Geology, 280, 168–181, 2011.

Sudhaus, H. and Sigurjón, J.: Improved source modelling through combined use of InSAR and GPS under consideration of correlated data errors: application to the June 2000 Kleifarvatn earthquake, Iceland, Geophys. J. Int., 176, 389–404, https://doi.org/10.1111/j.1365-246X.2008.03989.x, 2009.

Sun, T. and Wang, K.: Viscoelastic relaxation following subduction earthquakes and its effects on afterslip determination, J. Geophys. Res., 120, 1329–1344, https://doi.org/10.1002/2014JB011707, 2015.

Wigley, T. M. L. and Raper, S. C. B.: Thermal expansion of sea water associated with global warming, Nature, 330, 127–131, https://doi.org/10.1038/330127a0, 1987.

Wöppelmann, G. and Marcos, M.: Vertical land motion as a key to understanding sea level change and variability, Reviews of Geophysics, 54, 64–92, https://doi.org/10.1002/2015RG000502, 2016.

Wu, P.-C., Wei, M. M., and D'Hondt, S.: Subsidence in Coastal Cities Throughout the World Observed by InSAR, Geophysical Research Letters, 49, https://doi.org/10.1029/2022GL098477, 2022.

https://doi.org/10.5194/egusphere-2022-1113
Preprint. Discussion started: 27 January 2023

Xue, K., Wang, S., Hu, Y., and Li, M.: Creep Behavior of Red-Clay Under Triaxial Compression Condition, Frontiers in Earth Science, 7, https://doi.org/10.3389/feart.2019.00345, 2020.

Yao, Y., Cheng, H., Lin, J., and Ji, J.: Optimization of Burgers creep damage model of frozen silty clay based on fuzzy random particle swarm algorithm, Scientific Reports, 11, 18 974, https://doi.org/10.1038/s41598-021-98374-1, 2021.

Zou, L., Wang, S., and Lai, X.: Creep model for unsaturated soils in sliding zone of Qianjiangping landslide, Journal of Rock Mechanics and Geotechnical Engineering, 5, 162–167, https://doi.org/https://doi.org/10.1016/j.jrmge.2013.03.001, 2013.